Efficiency of SparkJet

M. Golbabaei-Asl, D. Knight⋆ and S. Wilkinson⋆⋆
⋆Rutgers, The State University of New Jersey
New Brunswick, New Jersey 08903, USA
⋆⋆NASA Langley Research Center
Hampton, Virginia 23681, USA

Abstract

The thermal efficiency of a SparkJet is evaluated by measuring the impulse response of a pendulum subject to a single spark discharge. The SparkJet is attached to the end of a pendulum. A laser displacement sensor is used to measure the displacement of the pendulum upon discharge. The pendulum motion is a function of the fraction of the discharge energy that is channeled into the heating of the gas (*i.e.*, increasing the translational-rotational temperature). A theoretical perfect gas model is used to estimate the portion of the energy from the heated gas that results in equivalent pendulum displacement as in the experiment. The earlier results from multiple runs for different capacitances of $C = 3, 5, 10, 20$, and 40μF demonstrate that the thermal efficiency decreases with higher capacitive discharges.[1] In the current paper, results from additional run cases have been included and confirm the previous results.

1. Introduction

The SparkJet™, pioneered by The John Hopkins University Applied Physics laboratory, is an electromagnetic local flow/flight control (ELFC) device.[2–8] The basic concept is illustrated in Fig. 1. A spark is discharged within a typical volume of several cm^3 (Stage 1). The high pressure gas discharges through a converging nozzle thereby generating an impulse (Stage 2). Provided there is a mechanism for recharging the gas in the cavity (Stage 3), the sequence can be repeated. Research on SparkJet has also been conducted at the University of Texas at Austin,[9] ONERA[10] and Rutgers University.[11]

The objective of the paper is to determine the thermal energy efficiency of a particular design of a SparkJet. The thermal energy efficiency is the fraction of the electrical energy which results in effective heating of the gas in the cavity.

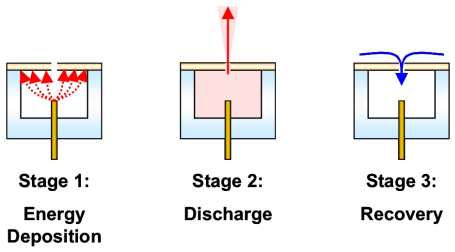

Figure 1: SparkJet[4]

2. Experiment

A brief description of the experimental apparatus is provided in the following sections. All the details are presented in the earlier paper by Golbabaei-Asl et al.[1]

2.1 Pendulum

To measure the impulse response of a single spark discharge, a prototype pendulum apparatus and SparkJet actuator was constructed.[1] The schematics of the pendulum apparatus is shown in Fig. 2 and the components include A. screw terminal block, B. connecting chains and wires, C. sharp carbide pins, D. stationary glass bearing surface, E. wood dowel, F. SparkJet actuator. The pendulum was a 12.7 mm diameter wooden (Maple) dowel mounted to a pivot block assembly on one end and to the SparkJet actuator on the opposite end. The pivot assembly consisted of a rectangular block of UHMW polyethylene ($19 \times 28 \times 63$ mm) with two sharp carbide scriber pins (from Moody Tools Model 51-1520) resting on hard glass surfaces.

The mass moment of inertia for a compound pendulum can be computed from the total rotating mass m (190.43 gram), the distance from the pivot axis to the center of the mass L_{cg} (291.4 mm), and the pendulum period T (1.5 s), *i.e.*, $I = mgL_{cg}(\frac{T}{2\pi})^2$ kg·m^2. A low torque electrical coupling was fabricated by suspending low stiffness conductors between two screw-terminal blocks, one attached to the stationary wooden support stand and the other to the rotating pivot block (See Fig. 2).

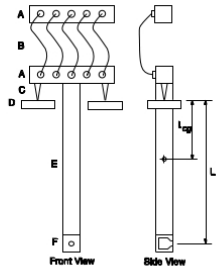

Figure 2: Pendulum Apparatus

2.2 SparkJet Actuator

A capacitive-discharge, ionization-triggered, tri-electrode SparkJet actuator was constructed.[1] Fig. 3 presents the schematics of the electrical circuit connected to the SparkJet. An ionization trigger was used to discharge the capacitor by introducing an approximately 1 microsecond pulse, V_p, into the step up transformer T to create a 25 kV pulse between nodes 5 and 3. The pulse was provided by a low cost, commercial trigger source (Information Unlimited, Model Ignitor10). Resistor R_2 helps to isolate the transformer from the spark gap while still allowing the ionization pulse to function. The circuit will function without R_2 but the influence of the transformer will be evident in the loop voltage measurements, particularly V_{12} and V_{34} complicating interpretation of the data. Diode D prevents reverse current and a second, echo discharge due to the collapsing magnetic field.

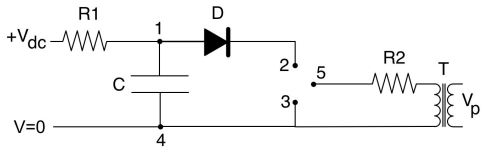

Figure 3: SparkJet electrical circuit schematic. V_{dc} = 550 volt unregulated, V_p trigger pulse from pulse generator, T pulse step up transformer, R_1 = 5 kOhm, R_2 = 1 kOhm, D diode (IN4007-30), C capacitor $(3, 5, 10, 20, 40\mu$F)

The high voltage trigger pulse creates an ionization channel between nodes 5 and 3 that subsequently allows the capacitor to discharge along path 1 – 2 – 5 – 3 (Fig. 4(b)). Fig. 4(c) shows the construction of the actuator.[1]

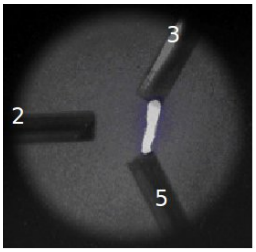

(a) Ionization trigger

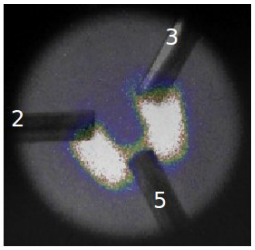

(b) Spark discharge

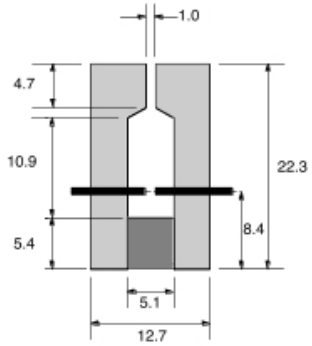

(c) Dimensioned cross-sectional diagram of SparkJet. All dimensions in millimeters.

Figure 4: SparkJet: a,b) photograph and c) diagram

2.3 Diagnostics

Since the maximum expected displacement of the pendulum was only a few tens of micrometers, it is important to accurately measure the displacement time history. A laser-based optical displacement sensor, Microepsilon optoNCDT model ILD-2200, was selected based on its range (2 mm), resolution (0.03 nm), stand-off distance (24 mm) and frequency response (20 kHz at −3 dB). The sensor has both analog and digital signal outputs. The analog output was used in this study.[1]

The instantaneous voltage across the gap and instantaneous loop current are measured in order to determine the input energy required to the main discharge spark. A large voltage drop is expected across both the supply and return legs of the wiring since the instantaneous current can be very high (on the order of 1000 amp). It was observed for a

particular implementation that roughly two-thirds of the capacitor voltage is dropped across the supply wiring. For this reason, a separate pair of voltage monitoring leads was attached directly to the actuator electrodes close to the spark gap.[1]

3. Theoretical Model

3.1 Model Description

The geometry of the pendulum is shown in Fig. 5. Prior to discharge and as a result of ambient noise the pendulum oscillates with small amplitudes. The discharge creates an air jet which generates a force and moves the pendulum. The geometry of the cavity is shown in Figure 6. The cavity is initially at ambient pressure p_∞ and ambient temperature T_∞. The energy deposited to the cavity, Q, is assumed to increase the temperature to T_{t_o} and pressure to p_{t_o} at a constant density ($\rho_{t_o} = \rho_\infty$) instantaneously at time t_0. An inviscid perfect gas model is assumed for the air flow to avoid elaborate computations required to account for thermochemical reactions.

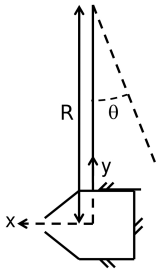

Figure 5: Pendulum configuration

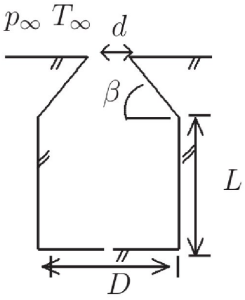

Figure 6: Cavity Geometry

3.2 Governing Equations

3.2.1 Pendulum Motion

Assuming that 1) the pendulum motion is planar, 2) the dimension of the SparkJet is small compared to the pendulum arm R, 3) the mass of the gas inside the SparkJet is negligible compared to the mass of the SparkJet (*i.e.*, $m_s(t)$ is constant), and 4) $\theta \ll 1$ radian; the pendulum motion can be simplified from Newton's second law

$$\frac{d^2\theta}{dt^2} + \omega^2\theta = \frac{R}{I}F(t) \tag{1}$$

where

$$\omega^2 = \frac{1}{I}\left[\int_0^R grdm_p + m_s gR\right] \tag{2}$$

where m_p is the mass of the pendulum (assuming a uniform density and constant cross section), $m_s(t)$ is the mass of the SparkJet, R is the distance from the pendulum pivot point to the cavity center, $F(t)$ is the force from the cavity exhaust, and I is the moment of inertia of the pendulum plus cavity system, *i.e.*,

$$I = \int_0^R r^2 dm_p + m_s(t)R^2 \tag{3}$$

3.2.2 Cavity Jet Flow

The initial total temperature of the gas in the cavity is

$$T_{t_o} = T_\infty + \frac{\eta Q}{\rho_\infty V c_v} \tag{4}$$

where ηQ is the effective heat added to the gas (*i.e.*, resulting in the increase in the translational-rotational temperature of the gas), ρ_∞ is the initial density of the gas in the cavity, V is the cavity volume and c_v is the specific heat at constant volume (see Fig. 6). The the subscript t_o indicates the total property of the gas at the time t_0. The quantity η is denoted the *thermal efficiency* of the SparkJet. The thermal efficiency in percent is $100 \times \eta$. The above expression may be rewritten as

$$T_{t_o} = T_\infty[1 + (\gamma - 1)\epsilon] \tag{5}$$

where

$$\epsilon = \frac{\eta Q}{p_\infty V} \tag{6}$$

For a physical interpretation of ϵ, see Anderson and Knight.[12]

Anderson and Knight have developed an analytical model to predict $F(t)$ in Eq. (1) for inviscid and perfect gas.[12] The force from the cavity is given by Eq. (7) assuming that the flow is initially sonic at the throat (see Anderson and Knight[12]).

$$\frac{F(t)}{p_\infty A} = \begin{cases} 0 & \text{for} \quad t < t_0 \\ c(\gamma)\left[1 + (\gamma - 1)\,\frac{Q\eta}{p_\infty V}\right][1 + \beta(t - t_0)]^{-\frac{2\gamma}{\gamma-1}} - 1 & \text{for} \quad t_0 \le t \le t_0 + \Delta t_1 \\ \left(\frac{2\gamma}{\gamma-1}\right)\left[\left(\frac{p_t}{p_\infty}\right)^{\frac{\gamma-1}{\gamma}} - 1\right] & \text{for} \quad t > t_0 + \Delta t_1 \end{cases} \tag{7}$$

where Q is the energy deposited into the cavity, V is the cavity volume, p_∞ is the ambient pressure, A is the cavity exit area, and η is the thermal efficiency. The energy deposition is assumed to occur instantaneously. The constants are given by the following relations

$$c(\gamma) = \left(\frac{2^\gamma}{\gamma + 1}\right)^{\frac{1}{\gamma-1}} \tag{8}$$

$$G = \left(\frac{2}{\gamma - 1}\right)\left(\frac{\gamma + 1}{2}\right)^{\frac{\gamma+1}{2(\gamma-1)}} \tag{9}$$

$$\beta = \frac{a_{t_o} A}{GV} \tag{10}$$

where a_{t_o} is the initial speed of sound in the cavity

$$a_{t_o} = \sqrt{\gamma R T_{t_o}} \tag{11}$$

and the initial temperature in the cavity can be found from Eq. (5)

The condition for initially sonic flow at the cavity exit (see Anderson and Knight[12]) is

$$\epsilon = \frac{Q\eta}{p_\infty V} > \frac{1}{\gamma - 1}\left[\left(\frac{\gamma + 1}{2}\right)^{\gamma/(\gamma-1)} - 1\right] \simeq 2.23 \text{ for } \gamma = 1.4 \tag{12}$$

The time interval Δt_1 of sonic flow at the cavity exit is

$$\Delta t_1 = 8.64\left(\frac{V}{a_{t_o} A}\right)\left[0.9129\left(1 + 0.4\frac{\eta\, Q}{p_\infty V}\right)^{1/7} - 1\right] \quad \text{for} \quad \gamma = 1.4 \tag{13}$$

The total pressure ratio to ambient pressure during subsonic flow at the cavity exit is determined by the following implicit equation[12]

$$\mu\sqrt{\mu^2 + 1}\left(2\mu^2 + 5\right) + 3\log\left(\mu + \sqrt{\mu^2 + 1}\right) - 3.946 + \left(\frac{8}{\sqrt{5}}\right)\left(\frac{a_{t_o} A}{V}\right)\frac{t - (\Delta t_1 + t_0)}{(1 + 0.4\epsilon)^{1/7}} = 0 \quad \text{for} \quad \gamma = 1.4 \tag{14}$$

where

$$\mu = \sqrt{\left(\frac{p_t}{p_\infty}\right)^{(\gamma-1)/\gamma} - 1} \tag{15}$$

For initially subsonic throat, $\epsilon < 2.23$, (see Anderson and Knight[12])

$$\frac{F(t)}{p_\infty A} = \left(\frac{2\gamma}{\gamma-1}\right)\left[\left(\frac{p_t}{p_\infty}\right)^{\frac{\gamma-1}{\gamma}} - 1\right] \tag{16}$$

The total pressure ratio to ambient pressure for subsonic throat is found by the following implicit relation

$$\mu\sqrt{\mu^2+1}(2\mu^2+5) + 3\log(\mu+\sqrt{\mu^2+1}) - \mu_0\sqrt{\mu_0^2+1}(2\mu_0^2+5) - 3\log(\mu_0+\sqrt{\mu_0^2+1}) + \frac{8}{\sqrt{5}}\frac{(\frac{a_{t_o}A}{V})(t-t_0)}{\sqrt{\mu_0^2+1}} = 0 \tag{17}$$

where μ is found by Eq. (15) and

$$\mu_0 = \sqrt{\left(\frac{p_{t_o}}{p_\infty}\right)^{(\gamma-1)/\gamma} - 1} \tag{18}$$

where

$$\frac{p_{t_o}}{p_\infty} = 1 + (\gamma-1)\epsilon \tag{19}$$

The total discharge time for initially sonic throat, $\epsilon > 2.23$, is

$$t_f = \frac{V}{a_{t_o}A}\left[8.99(1+0.4\epsilon)^{1/7} - 8.64\right] \tag{20}$$

and the total discharge time for initially subsonic throat, $\epsilon < 2.23$, is

$$t_f = (\frac{V}{a_{t_o}A})\frac{\sqrt{5}}{8}\left(\frac{p_{t_o}}{p_\infty}\right)^{1/7}\left\{\sqrt{\left(\frac{p_{t_o}}{p_\infty}\right)^{2/7} - 1}\left[2\left(\frac{p_{t_o}}{p_\infty}\right)^{3/7} + 3\left(\frac{p_{t_o}}{p_\infty}\right)^{1/7}\right] + 3\log\left[\left(\frac{p_{t_o}}{p_\infty}\right)^{1/7} + \sqrt{\left(\frac{p_{t_o}}{p_\infty}\right)^{2/7} - 1}\right]\right\} \tag{21}$$

where ϵ and $\frac{p_{to}}{p_\infty}$ are given by Eq. (5) and (19), respectively.

3.3 Numerical Method

The energy efficiency η is determined by choosing the value that creates a match between theoretical displacement and experimental displacement. The governing equation (Eq. (1)) is second order in time and is solved by a fourth order Runge-Kutta scheme.[13] The scheme incorporates variable time steps for different phases of pre-discharge, discharge (sonic and subsonic throat intervals), and post-discharge. Newton's method is used to find the numerical roots of the implicit relations (Eq. (14) and (17)) to determine $F(t)$. The two initial conditions, *i.e.*, the angle θ and the angular velocity $d\theta/dt$ at the instant of spark discharge are obtained from the experiment as well as the natural frequency ω.

4. Results

Experimental and theoretical results for one run of each capacitive discharges, *i.e.*, $C = 3, 5, 10, 20$, and 40 μF are shown in Fig. 7. The graphs present the pendulum displacement upon a single SparkJet discharge. The values of computed efficiency is given for all the cases (Fig. 7). It is worth to note that the experimental and computed results are particular of this specific SparkJet design.

The average efficiency and standard deviation values of multiple runs (5 to 10) for different capacitances are summarized in Fig. 8(a). The average efficiency and standard deviation values for different values of dimensionless deposited energy are plotted in Fig. 8(b). The results indicate lower efficiencies with higher capacitances, *i.e.*, capacitive discharges which lead to initially sonic throat conditions in the cavity.

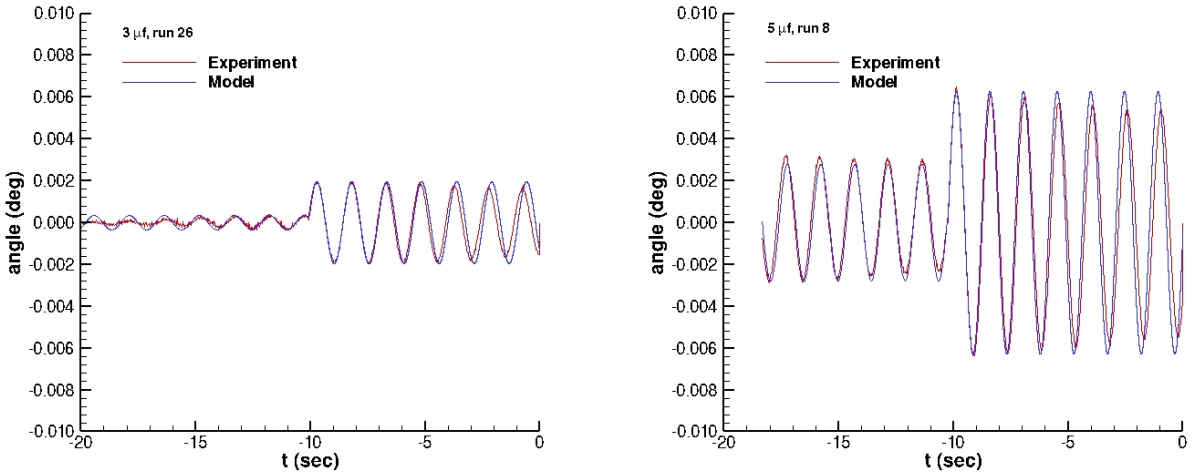

(a) η = 8.91% and Q = 181 mJ

(b) η = 7.82% and Q = 285 mJ

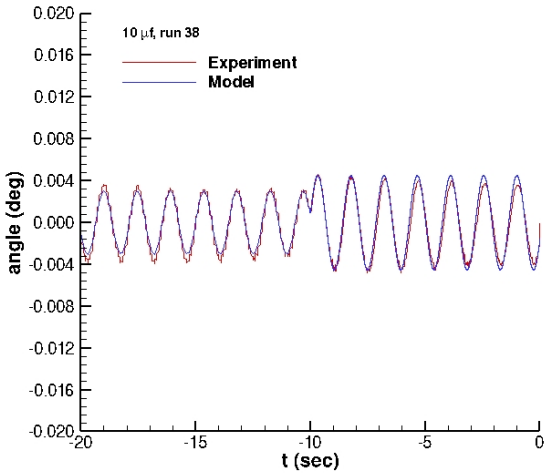

(c) η = 5.64% and Q = 572 mJ

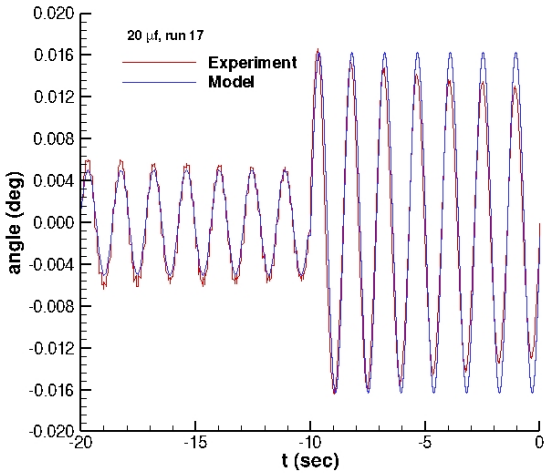

(d) η = 4.72% and Q = 1130 mJ

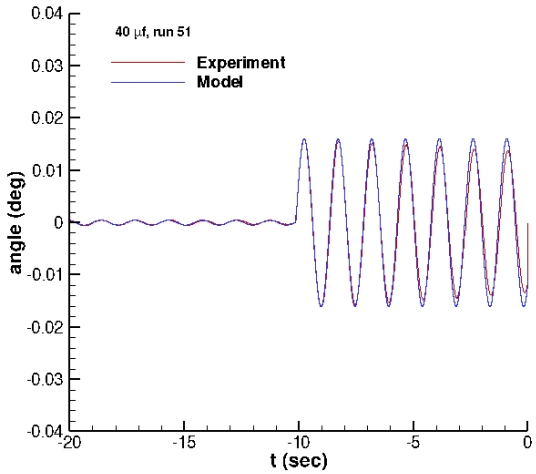

(e) η = 3.97% and Q = 1901 mJ

Figure 7: Experiment *vs* theory

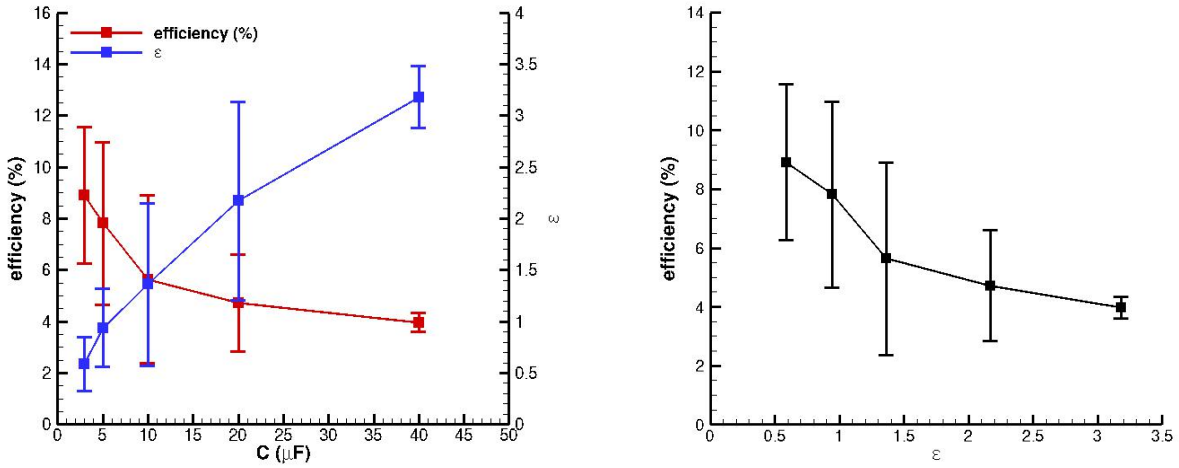

(a) η and ϵ *vs.* C

(b) η *vs.* ϵ

Figure 8: Thermal efficiency and dimensionless energy deposition parameter

5. Conclusion

A novel method for determining the thermal efficiency of the SparkJet is proposed. The thermal efficiency is the fraction of the capacitive discharge energy which is channeled into heating of the gas (*i.e.*, increasing the translational-rotational temperature). A SparkJet is attached to the end of a free swinging pendulum. The displacement of the pendulum *vs* time due to a single SparkJet discharge is measured using a laser displacement sensor. A theoretical model for the SparkJet thermal efficiency is developed assuming a perfect gas. The thermal efficiency of the SparkJet is calculated by fitting the predicted displacement *vs* time with the experiment. The results indicate less than 10% efficiency depending on the capacitance size. The thermal efficiency decreases with larger energy deposition magnitudes.

Acknowledgments

The theoretical portion of this research is supported by the US Air Force Office of Scientific Research under Grant FA9550-10-1-0111, managed by Dr. John Schmisseur, and the experimental portion by NASA Langley Research Center under Space Act Agreement SAA1-1360.

References

[1] Golbabaei-Asl, M., Knight, D., Anderson, K. and Wilkinson, S. SparkJet Efficiency. In: *51st AIAA Aerospace Sciences Meeting* , AIAA Paper 2013-0928, January 2013.

[2] Grossman, K., Cybyk, B., Rigling, M., and Van Wie, D. SparkJet Actuators for Flow Control. In: *41st AIAA Aerospace Sciences Meeting*, AIAA Paper 2003-0057, January 2003.

[3] Cybyk, B., Grossman, K., Wilkerson, J., Chen, J., and Katz, J. Single-Pulse Performance of the SparkJet Flow Control Actuator. In: *43rd AIAA Aerospace Sciences Meeting*, AIAA Paper 2005-0401, January 2005.

[4] Cybyk, B., Simon, D., Land, H., Chen, J., and Katz, J. Experimental Characterization of a Supersonic Flow Control Actuator. In: *44th AIAA Aerospace Sciences Meeting*, AIAA Paper 2006-0478, January 2006.

[5] Cybyk, B., Wilkerson, J., and Simon, D. Enabling High-Fidelity Modeling of a High-Speed Flow Control Actuator Array. In: *44th AIAA Aerospace Sciences Meeting*, AIAA Paper 2006-8034, January 2006.

[6] Haack, S., Land, B., Cybyk, B., Ko, H., and Katz, J. Characterization of a High-Speed Flow Control Actuator Using Digital Speckle Tomography and PIV. In: *4th AIAA Flow Control Conference*, AIAA Paper 2008-3759, June 2008.

[7] Haack, S., Taylor, T., Emhoff, J., and Cybyk, B. Development of an Analytical SparkJet Model. In: *5th AIAA Flow Control Conference*, AIAA Paper 2010-4979, June 2010.

[8] Haack, S., Taylor, T., Cybyk, B., Foster, C., and Alvi, F. Experimental Estimation of SparkJet Efficiency. In: *42nd AIAA Plasmadynamcis and Lasers Conference*, AIAA Paper 2011-3997, June 2011.

[9] Narayanswamy, V., Shin, J., Clemens, N., and Raja, L. Investigation of Plasma-Generated Jets for Supersonic Flow Control. In: *46th AIAA Aerospace Sciences Meeting*, AIAA Paper 2008-0285, January 2008.

[10] Caruana, D., Barricau, P., Hardy, P., Cambronne, J., and Belinger, A. The âPlasma Synthetic Jetâ Actuator - Aerother- modynamic Characterization and First Flow Control Applications. In: *47th AIAA Aerospace Sciences Meeting*, AIAA Paper 2009-1307, January 2009.

[11] Anderson, K. and Knight, D. Characterization of Single Pulse of Plasma Jet. In: *50th AIAA Aerospace Sciences Meeting*, AIAA Paper 2012-0188, January 2012.

[12] Anderson, K. and Knight, D. Plasma Jet for Flight Control. *AIAA Journal*, 50:1855-1872, 2012.

[13] Burden, R. and Faires, J. Numerical Analysis. Brooks/Cole Publishing Company, Pacific Grove, CA, USA, 1997.